Materials Advances

ROYAL SOCIETY OF CHEMISTRY

PAPER

View Article Online
View Journal | View Issue

Cite this: *Mater. Adv.*, 2025, 6, 5303

Biocatalytic application and structural elucidation of robust bacterial protein nanocages†

Ognjen Pećanac, ‡[a] Alexander Belyy, ‡*[b] Caterina Martin,[a] Rosalie Kleissen,[a] Marco W. Fraaije *[c] and Nikola Lončar *[a]

Received 23rd March 2025,
Accepted 24th June 2025

DOI: 10.1039/d5ma00268k

rsc.li/materials-advances

Encapsulins, bacterial protein nanocompartments, have emerged as promising platforms for enhancing biocatalyst stability. This study presents the identification and structural characterization of two encapsulins: ArthroEnc from *Arthrobacter* sp. SLBN-53 and DendroEnc from *Dendrosporobacter quercicolus*. Both bacterial encapsulins were successfully overexpressed in *Escherichia coli* and purified. Cryo-electron microscopy revealed that ArthroEnc assembles into a 20 nm T = 1 icosahedral capsid composed of 60 subunits, with its structure determined at 2.9 Å resolution, whereas DendroEnc forms a 40 nm T = 4 icosahedral complex with 240 subunits, resolved at 3.4 Å resolution. Both structures exhibit the characteristic HK97 phage-like fold. To explore their functional potential, the encapsulins were used to pack two distinct enzymes: CyanoPOX, a heme-containing peroxidase, and PTDH-mFMO, a fusion enzyme combining phosphite dehydrogenase with a flavin-containing monooxygenase. DendroEnc packed with CyanoPOX exhibited enhanced proteolytic stability, effectively shielding its cargo from chymotrypsin degradation. Activity assays with ABTS and guaiacol confirmed that encapsulated CyanoPOX retained enzymatic function within DendroEnc. Finally, mutating the pore of DendroEnc resulted in a fivefold reduction in activity, demonstrating the potential for tuning substrate diffusion. This study advances our understanding of encapsulin diversity and highlights their potential as versatile platforms for enzyme stabilization, biocatalytic and other biotechnological applications.

Introduction

Compartmentalization is a fundamental characteristic of all cells. It enables the segregation and coordination of physiological functions in a regulated and orderly manner.[1] To meet these diverse requirements, cells have evolved mechanisms that include lipid- and protein-based organelles.[2] Eukaryotic cells are primarily known for their reliance on lipid-based organelles, whereas prokaryotic cells predominantly employ protein-based compartmentalization strategies.[3,4] In the past, bacterial microcompartments have been recognized as the primary class of protein-based organelles in bacteria.[4] These large protein shells, often exhibiting a diameter larger than 100 nm, encapsulate and organize specific metabolic enzymes within a selectively permeable protein shell. This arrangement enhances reaction efficiency, sequesters toxic intermediates, and enables the development of new metabolic pathways in diverse bacterial species.[4,5] A little over a decade ago, a second extensive class of bacterial protein nanocompartments known as encapsulins was characterized.[6] Encapsulins are robust icosahedral protein structures formed *in vivo* through the self-assembly of 60 to 240 protomer subunits that exhibit the HK97 (Hong Kong 97) phage-like fold.[7] Structural analyses revealed that encapsulin protomers are composed of three highly conserved domains: the axial domain (A-domain), which forms the core of the subunit, the peripheral domain (P-domain), involved in inter-subunit interactions, and the extended loop (E-loop), which contributes to capsid assembly and stability.[6,8] Encapsulins typically range from 24 to 42 nm in diameter with different triangulation numbers (T = 1, T = 3, or T = 4).[9] A distinctive characteristic of encapsulins is their capability to encapsulate targeted cargo proteins, often enzymes.[10] This action is facilitated through a selective loading mechanism mediated by short targeting peptides located at the N- or C-terminus of a cargo protein.[11] Genes that encode cargo proteins and encapsulin are organized in a co-regulated operon that defines the encapsulin system.[12,13] The rationale governing the selective encapsulation of specific cargo proteins within bacterial microcompartments remains unclear. Predominant classes of cargo proteins identified within encapsulins include dye-decolorizing peroxidases (DyPs), ferritin-like proteins,

[a] *GECCO Biotech, Zernikepark 6, 9747 AN Groningen, The Netherlands. E-mail: n.loncar@gecco-biotech.com*
[b] *Membrane Enzymology, University of Groningen, Nijenborgh 3, 9747 AG Groningen, The Netherlands. E-mail: a.belyy@rug.nl*
[c] *Molecular Enzymology, University of Groningen, Nijenborgh 3, 9747 AG Groningen, The Netherlands. E-mail: m.w.fraaije@rug.nl*

† Electronic supplementary information (ESI) available. See DOI: https://doi.org/10.1039/d5ma00268k

‡ Equally contributed.

and some metalloenzymes, suggesting a potential functional relationship between these protein families and the encapsulin system.[10,14] A common characteristic observed among the identified cargo proteins appears to be their involvement in redox reactions,[15] leading to the hypothesis that encapsulins may play a crucial role in cellular detoxification mechanisms and oxidative stress management.[16,17] The inherent efficiency of encapsulins, coupled with their capacity to accommodate foreign cargo proteins,[18] makes them promising enzyme immobilizers with broad potential applications in fields of targeted therapeutics,[19] vaccine platforms,[20] and nanoscale bioreactors.[21]

This study reports on the structural and functional properties of two newly discovered bacterial encapsulins, named DendroEnc and ArthroEnc, from *Dendrosporobacter quercicolus* and *Arthrobacter* sp. SLB-53, respectively. Using cryo-electron microscopy (cryo-EM) and single-particle analysis we determined structures of a 240-subunit DendroEnc and a 60-subunit ArthroEnc, expanding our knowledge on structural diversity of encapsulins. We also demonstrate that DendroEnc effectively encapsulates a bacterial lactoperoxidase (CyanoPOX),[22] with further evidence showing that CyanoPOX retains its activity after encapsulation. Notably, proteolytic degradation studies show that once encapsulated, CyanoPOX exhibits resistance to chymotrypsin degradation. These findings suggest that DendroEnc has significant potential for stabilizing and protecting enzymes, offering exciting prospects for its application in various biotechnological fields.

Results and discussion

Identification of ArthroEnc and DendroEnc

To expand the diversity of available nanocompartments for biotechnological purposes, we conducted a genetic search for uncharacterized encapsulins using previously characterized encapsulins from *Mycolicibacterium hassiacum* (EncMh, WP_005630281.1)[10] and *Myxococcus xanthus* (EncA, WP_026114001)[23] as reference sequences. This resulted in the identification of a predicted protein (278 residues) from *D. quercicolus* that shared 47% sequence identity with EncA, and a predicted protein (265 residues) from *A.* sp. SLBN-53 that shared 83% sequence identity with EncMh. These respective genes were cloned in a pBAD vector for overexpression in *E. coli.* Successful overproduction of both proteins in *E. coli* was confirmed by SDS-PAGE analysis, which revealed prominent bands at the expected molecular weights for ArthroEnc (28.5 kDa) and DendroEnc (30 kDa) (Fig. S1, ESI†).

Development of ArthroEnc and DendroEnc as protein packaging systems

Expression and purification protocols for both ArthoEnc and DendroEnc were successfully established, yielding approximately 150 mg of encapsulins per liter of culture. To assess their potential for targeted protein encapsulation, we investigated the packaging of two distinct enzymes: CyanoPOX and PTDH-mFMO, which belong to different enzyme classes and require different cofactors. CyanoPOX, a heme-containing peroxidase from *Cyanobacterium* sp. TDX16, exhibits properties similar to bovine lactoperoxidase,[22] while PTDH-mFMO is a fusion enzyme combining phosphite dehydrogenase (PTDH) for cofactor regeneration with a flavin-containing monooxygenase from *Methylophaga* sp. (mFMO), capable of oxidizing indole to produce indigo dye.[24]

For targeted encapsulation, a 30-residue C-terminal peptide tag (PPPLPDSEPDREIPADDGSLGIGSLKGTRS), derived from a native dye-decolorizing peroxidase (DyP) of *Mycolicibacterium hassiacum*, was fused to each cargo enzyme.[10] Co-expression of encapsulins and cargo enzymes was achieved using a two-plasmid expression system, resulting in high expression levels of both encapsulins and their respective cargos. The optimized process yielded approximately 150 mg of each cargo-loaded encapsulin per liter of culture. SDS-PAGE analysis (Fig. S2, ESI†) of size-exclusion chromatography (SEC) fractions confirmed successful encapsulation, showing distinct bands corresponding to the encapsulin and cargo proteins-CyanoPOX (~60 kDa) and PTDH-mFMO (~100 kDa).

Structural elucidation of ArthroEnc and DendroEnc

To decipher the architecture of ArthroEnc and DendroEnc, purified samples were subjected to single-particle cryo-EM analysis. The structure of empty ArthroEnc was determined at 2.9 Å resolution. The structure revealed a spherical capsid with a diameter of 20 nm that is composed of 60 identical subunits, organized with the $T = 1$ icosahedral symmetry (Fig. 1A). Further structural analysis revealed that the ArthroEnc monomer adopts the characteristic HK97 phage-like fold, as described previously[7] (Fig. 1A). Electrostatic and hydrophobicity analysis of the encapsulin pore, formed by A-domains of 5 subunits, revealed a slightly positive surface charge on its outer side due to the presence of histidines and a ring of hydrophobic tyrosines on the inner side, potentially regulating pore function and substrate selectivity (Fig. 1C).

We then proceeded with structural analysis of DendroEnc and determined its structure at the resolution of 3.4 Å using single particle cryo-EM analysis. Our initial hypothesis, based on sequence similarity with previously studied encapsulins, suggested that DendroEnc forms a 180-subunit structure. However, cryo-EM revealed that DendroEnc assembles into a 40 nm 240-mer complex with $T = 4$ icosahedral symmetry (Fig. 1D). Within the asymmetric unit, four subunits exhibit minor structural differences in the A domain and E-loop, allowing them to fold into the large $T = 4$ icosahedral assembly (Fig. 1E).

Due to its structural organization, A-domains of DendroEnc form two types of pores, 5-fold and 6-fold, organized by 5 and 6 encapsulin subunits, respectively (Fig. 1F). The 6-fold pore, formed by hydrophilic asparagines and threonines and further stabilized by a ring of hydrophobic valines and phenylalanines, is nearly closed, limiting any transport through the encapsulin shell. In contrast, the 5-fold pore is more open and is composed of hydrophilic threonines and asparagines (Fig. 1G). In comparison to the analogical 5-fold pore of ArthroEnc (Fig. 1B), the pore of DendroEnc is 1 Å larger in diameter (10 Å) and does not have a hydrophobic interior (Fig. 1G). Interestingly, DendroEnc forms an additional triangular-shape pore at the interface of

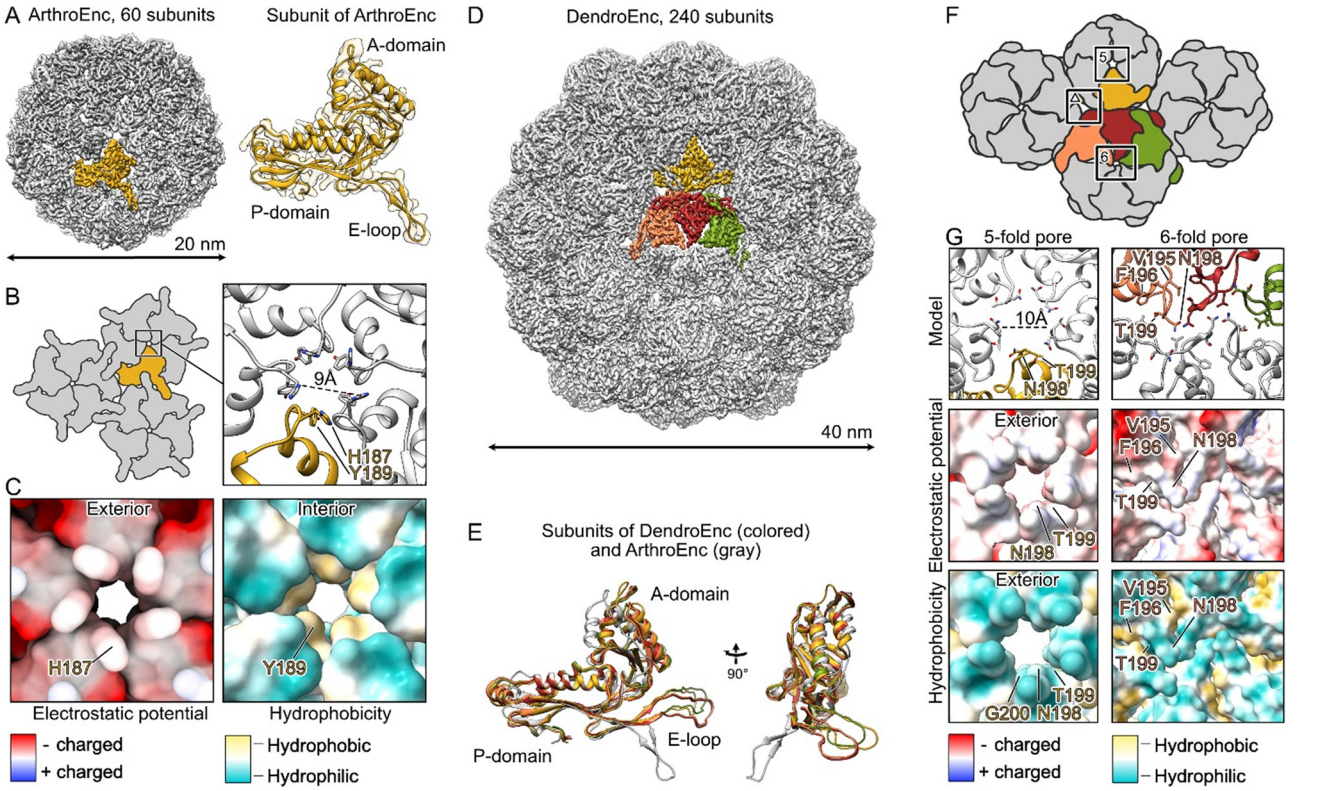

Fig. 1 Cryo-EM structures of ArthroEnc and DendroEnc encapsulins. (A) Cryo-EM reconstruction of ArthroEnc with $T = 1$ icosahedral symmetry with 60 subunits and a structure of its HK97-like fold domain. (B) Schematic organization of ArthroEnc and a close-up of its 5-fold pore. (C) Electrostatic surface and hydrophobicity of ArthroEnc's pore. (D) Cryo-EM reconstruction of DendroEnc revealing $T = 4$ icosahedral symmetry with 240 subunits. An asymmetric unit is shown in colors. (E) Structural alignment of four different subunits of DendroEnc (in orange, red, green and yellow) and a subunit of ArthroEnc (gray). (F) Schematic organization of DendroEnc and its 5-fold, 6-fold and triangular-shaped pores. (G) Structural organization of DendroEnc's 5- and 6-fold pores.

P-domains and E-loops of encapsulin subunits (Fig. 1F). This can be considered as a secondary entry point for substrate. Thus, DendroEnc pores are better designed to facilitate the transport of hydrophilic compounds, rendering it more suitable for potential biotechnological applications.

Proteolytic stability of DendroEnc constructs

Some encapsulins have been demonstrated to protect cargo proteins from proteolytic degradation.[10,25] To determine whether this applies to DendroEnc, we evaluated its ability to shield cargo proteins from protease activity. Incubation of empty DendroEnc and CyanoPOX-loaded DendroEnc with chymotrypsin, followed by SDS-PAGE analysis, demonstrated limited proteolytic degradation of the encapsulin shell (Fig. S3, ESI†). Additionally, the encapsulated CyanoPOX remained intact after 24 hours of chymotrypsin exposure, whereas non-encapsulated CyanoPOX was degraded. These results confirm the protective function of DendroEnc, further validating its ability to effectively encapsulate and safeguard cargo proteins.

Activity of DendroEnc CyanoPOX in the presence of ABTS and guaiacol

To evaluate whether CyanoPOX retained enzymatic activity when encapsulated within DendroEnc, two known substrates of this bacterial peroxidase,[22] ABTS (2,2′-azino-bis(3-ethylbenzothiazoline-6-sulfonic acid)) and guaiacol, were tested. DendroEnc CyanoPOX exhibited activity toward both substrates. At 10 mM, the activity for ABTS and guaiacol was 0.02 U mg^{-1} and 0.59×10^{-3} U mg^{-1} respectively. No detectable activity was observed in empty DendroEnc, confirming that the enzymatic activity originated solely from the encapsulated CyanoPOX. These results indicate that the pores of DendroEnc are sufficiently large to allow diffusion of relatively bulky substrates, such as ABTS, enabling efficient enzymatic catalysis within the nanocompartment. Table S4 and eqn (S1) (ESI†) outline the calculation procedure used to determine specific activity.

Engineering the 5-fold pore of DendroEnc

With established protocols for the recombinant production of DendroEnc carrying specific cargo, we explored the effects of modifying its pores. Structural insights into the DendroEnc pore architecture guided the design of a mutation aimed at narrowing or closing the pore. Using an encapsulated enzyme with substrates of varying sizes allowed us to assess the impact of this modification on substrate diffusion.

Specifically, we targeted residue N198, a key component of the 5- and 6-fold pores architecture (Fig. 1G). By substituting N198 with tryptophan, a bulky amino acid, we aimed to restrict

substrate entry into the encapsulin. Co-expression of the DendroEnc N198W variant with CyanoPOX successfully yielded CyanoPOX-loaded DendroEnc N198W. To assess the structural consequences of this mutation, we determined its structure to a 3.6 Å resolution using single-particle cryo-EM analysis, providing insights into the impact of pore engineering on encapsulin architecture.

Structural analysis of the DendroEnc N198W CyanoPOX complex revealed that, similar to wild-type DendroEnc, the 6-fold pore remains fully closed with a tight hydrophobic barrier (Fig. 2). Moreover, the introduction of tryptophan at position N198 resulted in a further reduction in the diameter of the 5-fold pore. The five tryptophan residues align precisely at the pore, constricting its diameter to 5 Å and effectively limiting molecular passage in and out of the encapsulin. Importantly, the N198W mutation did not change the overall architecture of encapsulin, showing its ability to tolerate significant mutations while preserving its integrity, further highlighting its potential for engineering tailored molecular gating properties.

The activity of the DendroEnc N198W CyanoPOX mutant was tested using ABTS as a substrate (0.004 U mg^{-1}), revealing a 5-fold reduction in activity compared to the CyanoPOX packed in wild-type DendroEnc. This decrease aligns with structural insights showing that the mutation reduced the diameter of the 5-fold pore.

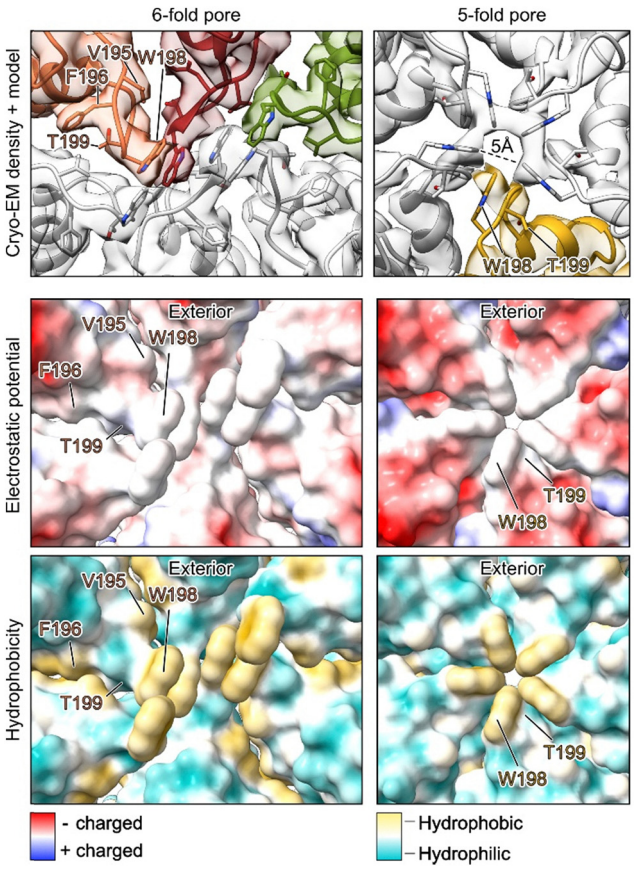

Fig. 2 Cryo-EM structure of the DendroEnc N198W CyanoPOX pores. The N198W mutation introduced a hydrophobic plug in the 6-fold pore and reduced the size of the 5-fold pore.

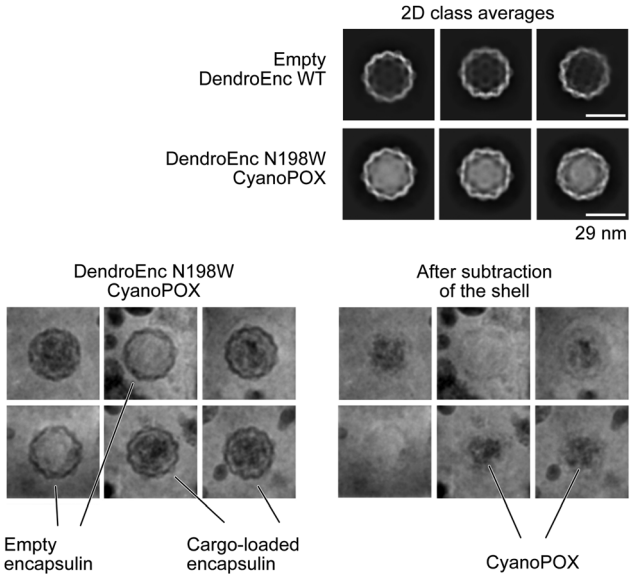

Fig. 3 2D class averages (above) of empty DendroEnc WT and DendroEnc N198W CyanoPOX and individual encapsulins DendroEnc N198W CyanoPOX with and without cargo (below).

Finally, to investigate the folding of CyanoPOX within DendroEnc, we compared 2D class averages of empty and cargo-loaded DendroEnc. This analysis enabled us to visualize the density corresponding to the encapsulated enzyme (Fig. 3), providing further confirmation of efficient cargo loading. However, the observed density appeared bulky and unstructured, with no indication of a defined symmetrical positioning of the cargo. Since the symmetry of the cargo might differ from that of the encapsulin shell, we performed shell subtraction to analyse the cargo alone. Further 2D classifications and 3D refinements did not reveal a clear structural organization, suggesting that the encapsulated enzymes do not adopt a fixed symmetrical arrangement within the encapsulin. These findings imply that CyanoPOX may remain in a flexible state inside DendroEnc.

Materials and methods

Chemicals and materials

The synthetic genes encoding for DendroEnc and ArthroEnc were ordered cloned in the pBAD vector (ampicillin resistance) from Twist Bioscience. The synthetic gene encoding for cargo proteins (CyanoPOX-cargo and PTDH-mFMO-cargo) were ordered at IDT (Integrated DNA Technologies). To prepare DendroEnc mutant, primers were ordered from Eurofins genomics. Superdex 200 Increase 10/300 GL column was purchased from Cytiva. Chymotrypsin from bovine pancreas and other chemicals were purchased from Sigma-Aldrich.

Cloning, protein co-expression and purification

IDT tools were used to codon optimize the sequences (Table S1, ESI†) that encode cargo enzymes (CyanoPOX-cargo and PTDH-mFMO-cargo) harboring a N-terminal 6×His-tag and the C-terminal targeting peptide to enable their expression in *E. coli*.

The targeting peptide used in this work belongs to a DyP-peroxidase[10] from the same operon as the encapsulin gene. These synthetic genes were cloned in pET vector (kanamycin resistance) using the Golden Gate methodology.[26] 5 μg of the cargo and encapsulin PCR mixtures were added to 50 μL $RbCl_2$ competent *E. coli* BL21-AI cells. The cells were left to incubate on ice for 30 min followed by the heat shock for 45 seconds at 42 °C. After the heat shock, the cells were placed on ice for another 3 minutes. 500 μL of SOC media was used to recover the cells. They were then placed in the thermal shaker at 37 °C for 45 min, 700 rpm. 100 μL of the cell mixture was spread onto the LB agar plates containing 100 μg mL^{-1} ampicillin and 50 μg mL^{-1} kanamycin. LB agar plates were placed into an incubator at 37 °C overnight. Overnight cultures were grown in 5 mL LB medium that was supplemented with 100 μg mL^{-1} ampicillin and 50 μg mL^{-1} kanamycin and were incubated at 37 °C, 135 rpm. Terrific Broth medium (500 mL), supplemented with 100 μg mL^{-1} ampicillin and 50 μg mL^{-1} kanamycin was used for the expression. Cultures were incubated at 37 °C, 135 rpm in baffled flasks until the OD_{600} reached ~0.75.

Expression of cargo enzymes and encapsulins was induced by adding IPTG (1 mM final concentration) and L-arabinose (0.02% final concentration). 5-Aminolevulinic acid (1 mM, final concentration) and iron sulfate (1 mM, final concentration) were added to the cultures containing CyanoPOX cargo in order to facilitate the biosynthesis of heme. Cultures were incubated at 24 °C at 135 rpm for 48 hours. They were then harvested by centrifugation (3700 rpm, 40 minutes, 4 °C). Cell pellets were resuspended in 35 mL lysis buffer (50 mM KPi, 150 mM NaCl, pH 7.5) and were sonicated on ice (5 s on 5 s off, 10 minutes, 70% amplitude). Cleared cell free extract was obtained by centrifugation at 12 000 rpm for 45 minutes at 4 °C. For precipitation of encapsulin-cargo constructs, equal volumes of cell free extract were mixed on ice with equal volumes of 12% PEG-8000, 50 mM KPi, pH 7.5, 2 M NaCl (used for ArthroEnc constructs) and 8% PEG-8000, 50 mM KPi pH 7.5, 2 M NaCl (used for DendroEnc constructs). The obtained solutions were incubated for 4 hours at 4 °C followed by centrifugation at 12 000 rpm for 45 minutes at 4 °C. The obtained pellets were resuspended in 50 mM KPi, 150 mM NaCl, pH 7.5. The resuspended mixture was selectively loaded onto Ni Sepharose gravity columns containing 3 mL resin in order to remove the excess unencapsulated cargo-enzyme.

Size exclusion chromatography (SEC) was used with the intention of further polishing encapsulins. A Superdex 200 increase 10/300 GL column with 20 mM KPi, 150 mM NaCl, pH 7.5 was used. Wavelengths were set at 280 nm and 420 nm corresponding to standard protein and cargo absorbance respectively. Fractions corresponding to the peak containing both wavelengths were pulled together and the SDS-PAGE analysis was then performed to assess the purity of encapsulins (Fig. S2 and S3, ESI†).

Cryo-EM, data analysis, model building

3 μl of encapsulins at concentrations 3 to 6 mg mL^{-1}, were applied onto a freshly glow-discharged copper R2/1 300 mesh grid (Quantifoil), blotted for 3 s on both sides with blotting force 0 and plunge-frozen in liquid ethane using the Vitrobot Mark IV system (Thermo Fisher Scientific) at 13 °C and 100% humidity.

Datasets were collected using a Talos Arctica transmission electron microscope (Thermo Fisher Scientific) equipped with an XFEG at 200 kV using the automated data-collection software EPU version 2.7 (Thermo Fisher Scientific). 2 images per hole with defocus range of −0.5 to −2.5 μm were collected with K3 detector (Gatan) operated in super resolution mode. Image stacks with 50 frames were collected with the total exposure time of 3.5 s and total dose of 45 e^{-} $Å^{-2}$.

For ArthroEnc, 719 micrographs were used for data processing. After motion correction and CTF estimation performed in Relion version 3.1,[27] 42 006 particles were picked in crYOLO,[28] extracted with box size 330 and pixel size 1.04 in Relion version 3.1, and imported in CryoSPARC. 20 200 particles after 2D classification were used for *ab initio* 3D refinement with simultaneous sorting into 3 classes. One class with the largest number of particles, 15 677, was used for non-uniform 3D refinement with icosahedral (I) symmetry. The reconstruction and corresponding particle alignments were used for Bayesian polishing in Relion, followed by final non-uniform 3D refinement in CryoSPARC.

For WT DendroEnc, 4498 micrographs were used for data processing. After motion correction and CTF estimation performed in Relion version 3.1, 108 615 particles were picked in crYOLO,[28] extracted with box size 440 and pixel size 1.59 in Relion version 3.1, and imported in CryoSPARC. 14 526 particles after 2D classification were used for *ab initio* 3D refinement with simultaneous sorting into 3 classes. One class with the largest number of particles, 6765, was used for non-uniform 3D refinement with icosahedral (I) symmetry. These particles were subjected to one more round of 3D refinement with simultaneous sorting into 2 classes. The class with the largest number of particles, 4549, was used for non-uniform 3D refinement with icosahedral (I) symmetry. The reconstruction and corresponding particle alignments were used for Bayesian polishing in Relion, followed by final non-uniform 3D refinement in CryoSPARC.

Finally, for DendroEnc N198W, 8176 micrographs were used for data processing. After motion correction and CTF estimation performed in Relion version 3.1, 35 472 particles were picked in crYOLO, extracted with box size 440 and pixel size 1.59 in Relion, and imported in CryoSPARC. 15 958 particles after 2D classification were used for *ab initio* 3D refinement with simultaneous sorting into 3 classes. One class with the largest number of particles, 10 561, was used for non-uniform 3D refinement with icosahedral (I) symmetry. The reconstruction and corresponding particle alignments were used for Bayesian polishing in Relion, followed by one more *ab initio* 3D refinement with simultaneous sorting into 3 classes. The class with 3997 particles was used for the final non-uniform 3D refinement. To demonstrate encapsulation of DendroEnc with CyanoPOX, we performed particle subtraction in CryoSPARC using a mask covering the DendroEnc shell.

B-factor sharpened reconstructions of final refinements were used for model building. Alphafold 2[29] model predictions of encapsulins were fit into the experimental density in Isolde[30] and refined in Phenix.[31] The statistics presented in Table S3 (ESI†) was calculated by MolProbity.[32]

Proteolytic stability of DendroEnc constructs

To assess proteolytic resistance, purified DendroEnc encapsulin obtained after SEC and non-encapsulated CyanoPOX (both at 1 mg mL^{-1}) were tested for proteolytic resistance with chymotrypsin from bovine pancreas. The protease stock solution (40 U mL^{-1}) was prepared by dissolving bovine chymotrypsin in 100 mM Tris-HCl buffer (pH 7.8) with 10 mM $CaCl_2$. 25 μL of 1 mg mL^{-1} encapsulin or CyanoPOX was mixed with 475 μL of protease stock solution. The digestions were performed at 50 °C for 24 h. Samples were analyzed by SDS PAGE.

Activity of DendroEnc CyanoPOX constructs

Reactions with DendroEnc CyanoPOX (1 mg mL^{-1}) and DendroENC N198W CyanoPOX (1 mg mL^{-1}) were performed at 25 °C. Enzymatic reaction with guaiacol was tested at 10 mM concentration in a 50 mM KPi, 150 mM NaCl, pH 7.5, while ABTS was tested at 10 mM concentration in 50 mM KPi, 150 mM NaCl, pH 5.0. 0.5 mM of H_2O_2 was used in all of the reactions. Formation of oxidized products was monitored at different wavelengths on the BioTek Synergy HTX multi-mode microplate reader (ABTS ε_{420} = 36.0 mM^{-1} cm^{-1} and guaiacol ε_{470} = 26.6 mM^{-1} cm^{-1}).[22] Reaction rates were determined from the linear regions of the reaction curves.

DendroEnc N198W mutant generation

DendroEnc mutation was performed using the QuickChange method.[33] The 25 μL PCR mix contained the following components: 12.5 μL of PfuUltra II Hotstart PCR Master Mix, 1 μL of forward primer (10 μM), 1 μL of reverse primer (10 μM), 1 μL of plasmid (100 ng μL^{-1}), 0.4 μL of DMSO, and MQ water to a final volume of 25 μL.

Conclusions

This study advances the understanding of bacterial encapsulins and their potential applications in biocatalysis through the identification and characterization of two novel systems: ArthroEnc from *Arthrobacter* sp. SLBN-53 and DendroEnc from *Dendrosporobacter quercicolus*. Structural analyses revealed that ArthroEnc assembles into a 20 nm capsid with $T = 1$ icosahedral symmetry, while DendroEnc forms a larger 40 nm structure with $T = 4$ icosahedral symmetry. Functional characterization demonstrated that DendroEnc CyanoPOX exhibits enzymatic activity with ABTS and guaiacol substrates. Notably, DendroEnc displayed resistance to proteolytic degradation and protected encapsulated enzymes during 24 hours of exposure to chymotrypsin. Furthermore, the N198W mutation in DendroEnc, designed to modulate pore size, reduced substrate accessibility, resulting in a 5-fold decrease in enzymatic activity relative to the wild type. These findings expand the known diversity of encapsulin systems and highlight their potential as robust platforms for enzyme stabilization and biocatalysis, offering promising possibilities for future applications in nanoreactor design and biotechnology.

Author contributions

M. W. F. and N. L. conceived and supervised experiments. A. B. performed the structural characterization. O. P., C. M. and R. K. carried out the identification and biochemical characterization. O. P., A. B., N. L. and M. W. F. contributed in writing the manuscript and approve the final version of the manuscript.

Conflicts of interest

There are no conflicts to declare.

Data availability

Coordinates for the cryo-EM structures of ArthroEnc, WT DendroEnc and DendroEnc N198W have been deposited in the Electron Microscopy Data Bank under accession numbers EMD-52714, 52715 and 52716. The corresponding molecular models have been deposited at the wwPDB with accession codes PDB 9I8D, 9I8E and 9I8F. Other relevant data supporting the findings of this study are fully included within the main article and its ESI.†

Acknowledgements

O. P., M. W. F. and N. L. received funding from the European Union's Horizon 2020 research and innovation program under Grant Agreement 101000607 (Project OXIPRO). We acknowledge Dr Alessandro Boverio for useful discussions on encapsulin structures. We thank Artem Stetsenko, Roman Koning, and Frank Faas for help with cryo-EM data collection and Michiel Punter for maintaining the computing cluster. Cryo-EM data were collected at the electron microscopy facilities of the University of Groningen and Leiden University Medical Center, nodes of The Netherlands Electron Microscopy Infrastructure (NEMI).

References

1 J. A. Jones and T. W. Giessen, *Biotechnol. Bioeng.*, 2021, **118**, 491–505.
2 T. W. Giessen, *Annu. Rev. Biochem.*, 2022, **91**, 1–19.
3 C. Greening and T. Lithgow, *Nat. Rev. Microbiol.*, 2020, **18**, 677–689.
4 C. A. Kerfeld, C. Aussignargues, J. Zarzycki, F. Cai and M. Sutter, *Nat. Rev. Microbiol.*, 2018, **16**, 277–290.
5 N. W. Kennedy, C. E. Mills, T. M. Nichols, C. H. Abrahamson and D. Tullman-Ercek, *Curr. Opin. Microbiol.*, 2021, **63**, 36–42.
6 M. Sutter, D. Boehringer, S. Gutmann, S. Günther, D. Prangishvili, M. J. Loessner, K. O. Stetter, E. Weber-Ban and N. Ban, *Nat. Struct. Mol. Biol.*, 2008, **15**, 939–947.
7 W. R. Wikoff, L. Liljas, R. L. Duda, H. Tsuruta, R. W. Hendrix and J. E. Johnson, *Science*, 2000, **289**, 2129–2133.
8 E. Eren, N. R. Watts, F. Montecinos and P. T. Wingfield, *Biomolecules*, 2024, **14**, 624.

9 J. A. Jones, R. Benisch and T. W. Giessen, *J. Mater. Chem. B*, 2023, **11**, 4377–4388.
10 N. Lončar, H. J. Rozeboom, L. E. Franken, M. C. A. Stuart and M. W. Fraaije, *Biochem. Biophys. Res. Commun.*, 2020, **529**, 548–553.
11 T. W. Giessen, B. J. Orlando, A. A. Verdegaal, M. G. Chambers, J. Gardener, D. C. Bell, G. Birrane, M. Liao and P. A. Silver, *eLife*, 2019, **8**, e46070.
12 T. W. Giessen and P. A. Silver, *Nat. Microbiol.*, 2017, **2**, 17029.
13 R. J. Nichols, C. Cassidy-Amstutz, T. Chaijarasphong and D. F. Savage, *Crit. Rev. Biochem. Mol. Biol.*, 2017, **52**, 583–594.
14 R. Rahmanpour and T. D. H. Bugg, *FEBS J.*, 2013, **280**, 2097–2104.
15 C. A. McHugh, J. Fontana, D. Nemecek, N. Cheng, A. A. Aksyuk, J. B. Heymann, D. C. Winkler, A. S. Lam, J. S. Wall, A. C. Steven and E. Hoiczyk, *EMBO J.*, 2014, **33**, 1896–1911.
16 K. A. Lien, K. Dinshaw, R. J. Nichols, C. Cassidy-Amstutz, M. Knight and R. Singh, *et al.*, *eLife*, 2021, **10**, e74358.
17 J. M. Rodríguez, C. Allende-Ballestero, J. J. L. M. Cornelissen and J. R. Castón, *Nanomaterials*, 2021, **11**, 1467.
18 A. Tamura, Y. Fukutani, T. Takami, M. Fujii, Y. Nakaguchi and Y. Murakami, *et al.*, *Biotechnol. Bioeng.*, 2015, **112**, 13–20.
19 T. W. Giessen, *Curr. Opin. Chem. Biol.*, 2016, **34**, 1–10.
20 P. Lagoutte, C. Mignon, G. Stadthagen, S. Potisopon, S. Donnat, J. Mast, A. Lugari and B. Werle, *Vaccine*, 2018, **36**, 3622–3628.
21 A. V. Almeida, A. J. Carvalho and A. S. Pereira, *Coord. Chem. Rev.*, 2021, **448**, 214188.
22 O. Pećanac, C. Martin, S. Savino, H. J. Rozeboom, M. W. Fraaije and N. Lončar, *ChemBioChem*, 2024, **25**, e202400713.
23 E. Eren, B. Wang, D. C. Winkler, N. R. Watts, A. C. Steven and P. T. Wingfield, *Structure*, 2022, **30**, 551–563.
24 N. Lončar, H. L. van Beek and M. W. Fraaije, *Int. J. Mol. Sci.*, 2019, **20**, 6148.
25 A. N. Gabashvili, N. S. Chmelyuk, M. V. Efremova, J. A. Malinovskaya, A. S. Semkina and M. A. Abakumov, *Biomolecules*, 2020, **10**, 966.
26 C. Engler, M. Youles, R. Gruetzner, T. M. Ehnert, S. Werner, J. D. Jones, N. J. Patron and S. Marillonnet, *ACS Synth. Biol.*, 2014, **3**, 839–843.
27 J. Zivanov, T. Nakane, B. O. Forsberg, D. Kimanius, W. J. Hagen, E. Lindahl and S. H. Scheres, *eLife*, 2018, **7**, e42166.
28 T. Wagner, F. Merino, M. Stabrin, T. Moriya, C. Antoni, A. Apelbaum, P. Hagel, O. Sitsel, T. Raisch, D. Prumbaum, D. Quentin, D. Roderer, S. Tacke, B. Siebolds, E. Schubert, T. R. Shaikh, P. Lill, C. Gatsogiannis and S. Raunser, *Commun. Biol.*, 2019, **2**, 218.
29 J. Jumper, R. Evans, A. Pritzel, T. Green, M. Figurnov, O. Ronneberger, K. Tunyasuvunakool, R. Bates, A. Žídek, A. Potapenko, A. Bridgland, C. Meyer, S. A. A. Kohl, A. J. Ballard, A. Cowie, B. Romera-Paredes, S. Nikolov, R. Jain, J. Adler, T. Back, S. Petersen, D. Reiman, E. Clancy, M. Zielinski, M. Steinegger, M. Pacholska, T. Berghammer, S. Bodenstein, D. Silver, O. Vinyals, A. W. Senior, K. Kavukcuoglu, P. Kohli and D. Hassabis, *Nature*, 2021, **596**, 583–589.
30 T. I. Croll, *Acta Crystallogr., Sect. D: Struct. Biol.*, 2018, **74**, 519–530.
31 D. Liebschner, P. V. Afonine, M. L. Baker, G. Bunkóczi, V. B. Chen, T. I. Croll, B. Hintze, L.-W. Hung, S. Jain, A. J. McCoy, N. W. Moriarty, R. D. Oeffner, B. K. Poon, M. G. Prisant, R. J. Read, J. S. Richardson, D. C. Richardson, M. D. Sammito, O. V. Sobolev, D. H. Stockwell, T. C. Terwilliger, A. G. Urzhumtsev, L. L. Videau, C. J. Williams and P. D. Adams, *Acta Crystallogr., Sect. D: Struct. Biol.*, 2019, **75**, 861–877.
32 C. J. Williams, J. J. Headd, N. W. Moriarty, M. G. Prisant, L. L. Videau, L. N. Deis and V. Verma, *et al.*, *Protein Sci.*, 2018, **27**, 293–315.
33 T. A. Kunkel, *Proc. Natl. Acad. Sci. U. S. A.*, 1985, **82**, 488–492.